Journal of Mathematical Modeling and Fractional Calculus
https://acspublisher.com/journals/index.php/jmmfc
Received:05-02-2025, **Revised:** 06-03-2025
Accepted:14-04-2025, **Published:** 30-06-2025
https://doi.org/10.48165/jmmfc.2025.2102, 2(1),19-38.

Finite Volume Simulation of Nanofluid Heat Transfer with Free Slip Lubrication

Shahid Hasnain[a], Nawal Odah Al-Atawi[b], Muhammad Saqib[c]

[a]Department of Mathematics, University of Chakwal, Pakistan
[b]Department of Mathematics, King Abdulaziz University, Jeddah, Saudi Arabia
[c]Khawaja Fareed University of Engineering and Information Technology (KFUEIT), Pakistan
Corresponding author Email:m.saqib@kfueit.edu.pk

Abstract: This study numerically investigates the viscous heating mechanism in a nanofluid-filled cavity subjected to external forces applied to the top lid, combined with laminar mixed convection of the nanofluid. The vertical walls of the cavity are assumed to be insulated, non-conductive, and impermeable to mass transfer. The horizontal walls are differentially heated, with the lower wall maintained at a higher temperature while the upper wall remains cooler. The primary objective of this research is to introduce a novel method that accurately incorporates height in the solution of heat transfer equations, using transient analysis for numerical iterations. Although the fluid flow reaches a steady state, the square cavity's walls are fully insulated, and a constant heat flux is generated by the motion of the top lid. This work aims to analyze the effects of viscous heating in a fully insulated lid-driven cavity with Neumann boundary conditions under both no-slip and free-slip conditions, while varying Rayleigh and Prandtl numbers as independent parameters. The simulations are performed for a specific case where the Prandtl number $Pr = 6.2$ is fixed, while Rayleigh numbers and the volume fraction of the nanofluid (water mixed with copper nanoparticles) range from 0% to 5%. The time-dependent vorticity-stream function and thermal energy equations are discretized and solved using a custom finite volume method combined with the artificial compressibility approach, implemented in MATLAB. Despite viscous heating having a limited effect, the Neumann boundary conditions with no-slip and free-slip assumptions influence heat retention within the insulated cavity. The free-slip condition acts as a lubricant, leading to reduced temperature distribution, particularly under lower Rayleigh numbers and higher Prandtl numbers, compared to the no-slip condition. This is attributed to the free-slip effects under these conditions, which enhance heat dissipation and increase the fluid velocity, further stabilizing the system.

Keywords: Nanofluid; Mixed Convection; Free Slip Lubrication; FVM

1. Introduction

Studying fluid motion can be done in a domain that is either square, rectangular, or cubic. For the sake of backward compatibility, the viscous, non-variable density, fluids can be influenced by the simplest mechanical derivational force. A lid-driven square or cubic cavity has one wall moving tangentially towards the other bordering or immovable walls. Several scholars analyzed fluid flow problems using simple geometry. In which they performed simulations through experiments as well as numerical techniques for the investigation and validation of specific physical phenomena. Theoretically, there

is widespread agreement that the Navier Stokes (NS) equations represent the most basic mathematical model that can be used to explore the flow field of fluids. By connecting the NS equations with the stress tensors of relevant fluid models, it is possible to investigate both compressible and incompressible flow fields simultaneously [1, 2]. Shankar et al. [1] explored the two-dimensional steady or unsteady incompressible flow problems using an analytical and numerical set-up by taking into consideration the NS equations as the fundamental mathematical model. Later on, Burggraf [3] expanded the scope of his research to include numerical-analytical comparison. The efforts of Ghia et al. [4] marked the beginning of the search for precision and efficacy. A two-dimensional square cavity with the top wall moving with constant speed and steady nature of flow at Reynolds (Re) number up to 10^4 was estimated by Ghia et al. [4]. A series of experiments was carried out to analyze the flow inside the cavity with different aspect ratios in three dimensions. Several research groups have constructed and statistically analyzed three-dimensional test problems, leading to Deville et al. conclusions [5, 6, 7]. These results indicated that the spectral method improves the two-dimensional flow problem with more accuracy. These kinds of efforts provide beneficial results for two-dimensional unsteady NS equations, which are used to explore incompressible flow in lid-driven cavity problems, which goes on to become a benchmark in the filed [7]. These collaborative efforts have yielded conclusive results at $Re = 3200$. Therefore, their technique offers very exact numerical answers up to $Re = 10^3$. For $Re = 10^3$ Albensoeder used the method proposed by Botella and Peyret to obtain the extremely precise flow field over a range of cavity lengths with both rigid and periodic boundary conditions [8, 9, 10].

Additionally, lid-driven cavity flow dynamics entail a number of elementary phenomena from the field of fluid mechanics. Taylor [11] proposed the similarity solutions in which the Vortex problem is discussed at the edges of the domain, caused by the existence of discontinuous boundary conditions. A regularization or smoothing of the discontinuity might be thought of as an artifice that eliminates the singularity. An experimental implementation of the lid-driven cavity faces key challenges due to a pressure divergence at the singular corner. In addition, such discontinuity might result in pumping and leaking effects. One further oddity has to do with the viscous flow that occurs close to the acute corners that are formed by two walls that remain immovable. If the flow is confined at an angle, bifurcation which is known as Hopf bifurcation, in the driven cavity is observed [11, 12, 13, 14, 15]. In addition to numerical methods, other approaches, such as the bi-orthogonal series method and the usage of Green's functions, can be utilized in order to arrive at a resolution to issues of such nature. Prandtl-Batchelor theorem predicted that at high Reynolds numbers with no instabilities, the inviscid core of uniform vorticity for steady two-dimensional flow gives rise to building such a vortex. Thus, experiments and numerical analysis both back up, vortex patterns which are analyzed by computer simulations [15, 16, 17]. On the other hand, it has been seen that at large values of the Reynolds number, the steady two-dimensional flow is unstable. So, as the Re grows above a critical value, the cavity show vortices that are in smaller size downstream towards the moving wall. The coupling between velocity and pressure in the primitive variables can be transformed into discrete formulations to study incompressible NS equations, which plays an important role in the convergence of any numerical technique in fluid flow simulations. Additionally, the primitive variable (pressure) can be read by the equation of continuity. There is no well-defined, separate, mathematical equation that can be used to describe pressure which makes it hard to solve the incompressible NS equations [17, 18, 19, 20].

We quantitatively explore nanofluid laminar mixed convection in a square cavity. Insulated, non-conducting, mass-transfer-impermeable vertical walls are postulated. The Argonne National Laboratory research group studied the use of nanometer-sized particles for the first time on a regular basis more than a decade ago. The nanoparticles (typically between 1 and 100 nm in size) in a nanofluid are suspended in the base fluid by means of a well-crafted colloidal suspension. As opposed to the chemical instability of nanoparticles, which are typically composed of metals, metal oxides, or carbon, basic fluids like water, oil, and Ethylene Glycol serve as good examples of nanoparticles. This group may have been the first to call fluids with nanometer-sized particles nanofluids in 1995. He showed that heat was moved much faster when copper or aluminum nanoparticles were suspended in water or

other liquids [21, 22, 23]. A nanofluid is considered to be a single phase to study natural convection in a 2D cavity by using copper water nanofluid with different volumetric fractions of Cu nanoparticles in water which enhanced heat transfer for any Grashof number [21]. Nanofluids of copper-water and Al_2O_3-water rises the thermal conductivity by increasing the percentage of solid volume fraction which is suggested by Lee et al. [22]. He concluded that any new models of nanofluid thermal conductivity should include size, surface area-dependent functionality, and structure-dependent actions. Therefore, the convective heat transfer coefficient has been the subject of both theoretical and experimental research, some of which has been recorded [22, 23, 24, 25].

Sandeep et al. [26] examined the effects of a volume percentage of dust particles in an MHD nanofluid on the momentum and heat transfer behavior while the fluid was forced to flow over a stretching surface. They used a computational method based on the Runge-Kutta approximation to solve the differential equations. It revealed that fluid-particle interaction boosted heat transfer and reduced friction. When a Newtonian fluid is subjected to a mixed convection process involving multiple heat sources in a lid-driven cavity, Zhou et al. [27] looked at the Boussinesq approximation in the thermal energy equation. Rahman et al. [28, 29] found that the magnetic field and Joule heating of a lid-driven flow with a semi-circular heated wall are independent of viscous heating. The viscous terms used to calculate the meteorite's surface temperature are a part of the thermal energy calculation for a highly viscous flow. Future studies may explore Newtonian homogeneous and heterogeneous nanofluids as cavity-flow-occupied fluids with viscous heating and sliding effects [29, 30, 31, 32, 33, 34]. A square cavity filled with nano-fluids which consists of several nano-particles (water plus nano-particles of Cu, Ag, TiO_2 & Al_2O_3) along different wall conditions, give rise to uniform temperature distribution, is investigated by using finite volume methodology together with mesh independent scheme to get highly accurate solution of the coupled partial differential equations [35]. Tiwari et al. [36] investigated the nanofluid regime (nanoparticles of Copper & water) for a partially heated cavity with two-sided lids along the different directions of wall movement and controllable Richardson number. Nano-fluids features are analyzed by a number of factors such as various boundary conditions which are related to temperature, volume fractions of different solid nano-particles, Rayleigh number effects, average Nusselt number, and partitions of locations. This yields enclosure heat transfer correlations for different thermal boundary conditions as well as source terms for various wall settings to investigate the natural convection phenomena using water base nanofluids. This is done so that the nanofluids can cool the heat source more effectively, within a nanofluid-filled container that oscillated in heat flow, periodic natural convection was an idea that was considered by certain researchers. In buoyancy-driven flow in a cavity, non-uniform surface heating affects flow and heat transfer, and it is used in crystal development in liquids, energy storage, geophysics, solar distillers, and other fields [32, 33, 35, 36]. In order to maximize and enhance the amount of heat that is transferred by natural convection within a square closed cavity.

Although a significant amount of work has been devoted to investigating situations of the square as well as rectangular cavities filled with nanofluid, very few works have concentrated on the investigation of numerical discretization. In order to tackle problems involving conductive heat transfer, convective heat transfer, or a mixture of the two into regular geometries, for the purpose of solving the Navier-Stokes equation in enclosures while taking into account the energy equation, more specific order four algorithms have been utilized. The creation of a novel strategy for the solution of heat transfer equations including convection is the purpose of this body of work. The novel method uses a staggered grid approach with finite volume and combines it with artificial compressibility. Therefore, such demonstration of the usefulness of the method and to gain an understanding of how the natural convection mechanism is affected when nanofluids are present in closed square systems. Patankar et al. [14] introduced the first attempt at the segregated method in which pressure is computed in two steps; first find the intermediate value for the velocity field from the guess pressure value while in 2nd step, the computed value can be validated through continuity equation. The absence of a time derivative for the pressure variable in the continuity equation makes it more difficult. Addressing such

difficulty in terms of time derivative pressure in the continuity equation is the collateral objective of the current article. The methods increase the stability of the pressure solver, which in turn improves the whole method's performance. A major problem with these approaches is that they do not impose a connection between velocity and pressure throughout the linearized system's solution. This slows down convergence as the number of grid points rises. The numerical approach is the backbone of this simplest but most complicated (in terms of numerical) problem. The originality of the issue involves the following;

1. The assessment of the Kinetic energy,
2. The derivation to Vorticity Stream function,
3. Finite Volume staggered grid approach,
4. Weak Compressibility.

The motivation for the current study started in the introduction section while the assessment of Kinetic energy is done in section 2. A brief description of mathematical modeling is introduced in section 3 which then derives the governing system with specific boundary conditions. Section 4 vorticity Stream function technique is discussed. Following that, section 5 gives a short description of the finite difference (FD) method, followed by staggered grid finite volume (FV) and Weak (Artificial) Compressibility approaches. This section overviews numerical approaches for the approximation of functions and derivatives. In section 6, an analysis of the article results is discussed.

2. Kinetic Energy of Incompressible Flow

Fluids, in contrast to gases, cannot be compressed unless very large forces are applied to them. As a result, the behavior of a fluid is very similar to that of an incompressible material namely, $div\,\overline{U} = 0$, and the continuity equation transforms to an equation for the transfer of density, i.e

$$\frac{\partial \rho}{\partial t} + \overline{U}.\bigtriangledown \rho = 0. \tag{1}$$

The equations whose numerical solutions will be discussed in more depth in the next sections. We also make the assumption that the density of the fluid remains the same throughout time ($\rho = \rho_0 = 1$). This is the common assumption for many different types of fluids, including oil or water. After that, we have the following incompressible Navier Stokes equations;

$$\frac{\partial \overline{U}}{\partial t} + \underbrace{(\overline{U}.\bigtriangledown)\overline{U}}_{\text{Convection}} = -\frac{1}{\rho_0}\bigtriangledown \mathbb{P} + \nu \underbrace{\triangle \overline{U}}_{\text{Diffusion}} + \mathbb{F}_{forces}, \tag{2}$$

$$div\,\overline{U} = 0. \tag{3}$$

Where $\nu = \dfrac{\mu}{\rho_0}$ in equation (2). Also, density is constant which is in normalized form.

$$\overline{U} = 0, \quad at \;\; Boundary$$
$$\overline{U}(0) = \overline{U}_0, \quad in \;\; Domain$$

Therefore, the kinetic energy of the fluid is defined by the following relation,

$$Energy_{kinetic}(t) = \frac{1}{2}\int_{Domain} |\overline{U}|^2 dx. \tag{4}$$

Time derivative is provided by when there are no volumetric forces.

$$\frac{d}{dt}Energy_{kinetic}(t) = \int_{Domain} \overline{U}\ \overline{U}_t dx. \tag{5}$$

In connection to equation (2), we can write.

$$\frac{d}{dt}Energy_{kinetic}(t) = \int_{Domain} \overline{U}\ (-\underbrace{(\overline{U}.\bigtriangledown)\overline{U}}_{\text{Convection}} - \bigtriangledown \mathbb{P} + \nu \underbrace{\triangle \overline{U}}_{\text{Diffusion}})dx.$$

$$\frac{d}{dt}Energy_{kinetic}(t) = -\int_{Domain} \overline{U}\ (\overline{U}.\bigtriangledown)\overline{U})dx - \int_{Domain} \overline{U}(\bigtriangledown \mathbb{P})dx + \nu \int_{Domain} \overline{U}(\triangle \overline{U})dx. \tag{6}$$

A detailed description of each term can be followed by Gauss's theorem;

$$\left.\begin{aligned} \int_{Domain} \overline{U}\ (\overline{U}.\bigtriangledown)\overline{U})dx &= \frac{1}{2}\int_{Domain} \overline{U} \bigtriangledown (|\overline{U}|^2)dx - \int_{Domain} \underbrace{\overline{U}.(\overline{U} \times rot\ \overline{U})}_{=0} dx. \\ \int_{Domain} \overline{U}\ (\overline{U}.\bigtriangledown)\overline{U})dx &= \frac{-1}{2}\int_{Domain} \underbrace{(div\ \overline{U})}_{=0}(|\overline{U}|^2)dx + \frac{1}{2}\int_{Domain} (|\overline{U}|^2)\underbrace{(\overline{U}.n)}_{=0} ds. \end{aligned}\right\} \tag{7}$$

which shows that 1st term in equation (5) is zero,

$$Term_1 = \int_{Domain} \overline{U}\ (\overline{U}.\bigtriangledown)\overline{U})dx = 0. \tag{8}$$

$$\int_{Domain} \overline{U} \bigtriangledown \mathbb{P}dx = \int_{Domain} \underbrace{(div\ \overline{U})}_{=0} \mathbb{P}dx + \int_{Boundary} \mathbb{P}.\underbrace{(\overline{U}.n)}_{=0} ds$$

which shows that 2nd term in equation (5) is zero,

$$Term_2 = \int_{Domain} \overline{U} \bigtriangledown \mathbb{P}dx = 0. \tag{9}$$

For further information, let us look again equation (6),

$$\frac{d}{dt}Energy_{kinetic}(t) = \nu \int_{Domain} \overline{U}(\triangle \overline{U})dx.$$

$$\frac{d}{dt}Energy_{kinetic}(t) = \nu \int_{Domain} \overline{U}_1(\triangle \overline{U}_1)dx + \nu \int_{Domain} \overline{U}_2(\triangle \overline{U}_2)dx + \nu \int_{Domain} \overline{U}_3(\triangle \overline{U}_3)dx.$$

Again by applying Gauss's theorem,

$$\frac{d}{dt}Energy_{kinetic}(t) = \nu \sum_{n=1}^{3}(-\int_{Domain} (|\bigtriangledown \overline{U}_n|^2 dx + \int_{Boundary} \overline{U}_n \underbrace{(\bigtriangledown \overline{U}_n.n)}_{=0} ds), \frac{d}{dt}Energy_{kinetic}(t), \tag{10}$$

$$\frac{d}{dt}Energy_{kinetic}(t) = -\nu \sum_{n=1}^{3} \int_{Domain} (|\bigtriangledown \overline{U}_n|^2 dx \leq 0. \tag{11}$$

As a direct result of equation (10), the amount of the kinetic energy of the fluid that is transferred reflects the losses which are occurring as a result of friction present in a viscous flow.

3. Mathematical formation to governing system

Consider a square cavity filled with a nanofluid and assumed that the vertical walls are insulating, non-conducting, and impervious to the movement of mass with differential heating on the horizontal wall at a hot condition (bottom wall), while the top wall is kept at a colder temperature, see Figure 2. The nanofluid contained within the enclosure exhibit Newtonian behavior with incompressible nature and has a laminar flow. It is presumed that the nanoparticles have a shape and size that are both consistent with one another. In addition to this, it is also considered, the fluid phase and the nanoparticles are both in a condition of thermal equilibrium and that they are moving at the same velocity. We have looked at the continuity, momentum, and energy equations for an unsteady flow in two dimensions governed by a Newtonian fluid with a Fourier constant feature. Henceforth, the amount of heat transferred between sides by radiation is insignificant in comparison to the amount transferred via other means of heat transfer. The two-dimensional, unsteady, and incompressible NS (Navier-Stokes) equations for flow with the assumption that the thermal characteristics remain the same, are as follows:

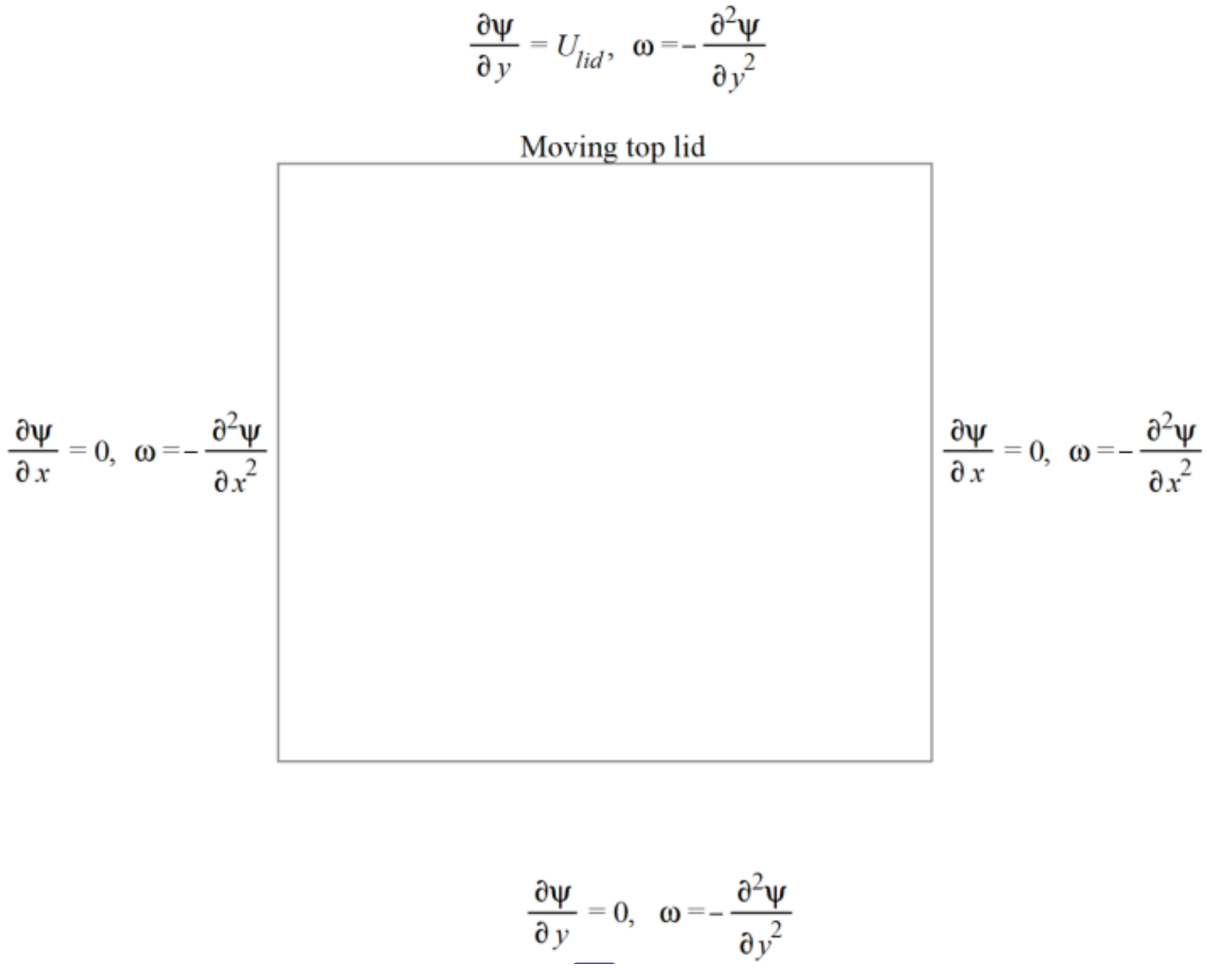

Figure 1: shows with Cartesian coordinates, a two-dimensional model of lid-driven cavity flow.

x-directional Momentum:

$$\rho_{nf}(\overline{u}_{\overline{t}} + \overline{u}\overline{u}_{\overline{x}} + \overline{v}\overline{u}_{\overline{y}}) = -\overline{p}_{\overline{x}} + \mu_{nf}(\Delta^2 \overline{u}) + \underbrace{\mathbb{F}_{forces}}_{=0}, \tag{12}$$

y-directional Momentum:

$$\rho_{nf}(\overline{v}_{\overline{t}} + \overline{u}\overline{v}_{\overline{x}} + \overline{v}\overline{v}_{\overline{y}}) = -\overline{p}_{\overline{y}} + \mu_{nf}(\Delta^2 \overline{v}) + g\overline{T}((1-\varphi)\rho_f \beta_f + \varphi \rho_s \beta_s), \tag{13}$$

Equation for Energy:

$$\overline{T}_{\bar{t}} + \overline{u}\overline{T}_{\bar{x}} + \overline{v}\overline{T}_{\bar{y}} = \frac{K_{eff}}{(\rho C_p)_{nf}}(\Delta^2 \overline{T}). \tag{14}$$

3.1. Thermophysical properties of the regular nanofluid

Furthermore, μ_{nf}, ρ_{nf}, $(\rho C_p)_{nf}$ and k_{nf} are the nanofluids values for its dynamic viscosity, density, heat capacity, and the thermal conductivity respectively where the equations to evaluate their thermophysical characteristics are provided in the following Table 1.

Properties	**Nanofluid**	**Pure Water**
Dynamic Viscosity	$\mu_{nf}=\frac{\mu_f}{(1-\varphi)^{2.5}}$	–
Effective Density of nanofluid	$\rho_{nf}= (1-\varphi)\rho_f + \varphi\rho_s$	ρ_{nf}(kg/m^3)=997.7
Heat capacity of nanofluid	$(\rho C_p)_{nf}=(1-\varphi)(\rho C_p)_f + \varphi(\rho C_p)_s$	C_p(J/kg.K)=4179
Effective Thermal Conductivity of nanofluid	$k_{nf}=\frac{k_s+2k_f-2\varphi(k_f-k_s)}{k_s+2k_f+\varphi(k_f-k_s)(k_f)}$	K(W/m.K)=0.613

Table 1: Thermophysical properties of the regular nanofluid [37].

3.2. Non-dimensionalization technique

We introduce the non-dimensionalization technique to the system in equations (12– 14), in the following way,

$$x=\frac{\overline{x}}{L},\ y=\frac{\overline{y}}{L},\ u=\frac{\overline{u}L}{\nu_f},\ v=\frac{\overline{v}L}{\nu_f},\ t=\frac{\overline{t}}{\tau},\ \tau=\frac{t}{L^2/\nu_f},\ p=\frac{\overline{p}}{\widetilde{p}},\ \widetilde{p}=\frac{\rho_f \nu_f^2}{L^2},\ \&\ \Theta=\frac{\overline{T}-\overline{T}_c}{\overline{T}_h-\overline{T}_c}. \tag{15}$$

Such transformation 15 leads to the following non-dimensional numbers, which are

$$Ra = g\beta_f L^3 \frac{\overline{T}_h-\overline{T}_c}{\nu_f \alpha},\ \&\ Pr=\frac{\nu_f}{\alpha_f}. \tag{16}$$

3.3. Governing system

It has been determined that the equation that Brinkman provided should be utilized as the relation for effective viscosity in which experimentally measured the apparent viscosity of the transformer oil-water nanofluid and of the water-copper nanofluid in the temperature range of 20^0C – 50^0C. The experimental results reveal relatively good agreement with Brinkmans theory [38, 39, 41, 42]. Therefore, the proposed governing system which consists of continuity, momentum, and energy equations can be used to get an analysis of unsteady laminar flow. Hence, we have the following system:

$$\left.\begin{aligned} \rho_{nf}(u_t + uu_x + vu_y) &= -p_x + \mu_{nf}(\Delta^2 u),\\ \rho_{nf}(v_t + uv_x + vv_y) &= -p_y + \mu_{nf}(\Delta^2 u) + \frac{Ra}{\beta_f Pr}\Theta((1-\varphi)\rho_f\beta_f + \varphi\rho_s\beta_s),\\ \Theta_t + u\Theta_x + v\Theta_y &= \frac{\alpha_{nf}}{\alpha_f Pr}(\Delta^2\Theta). \end{aligned}\right\} \tag{17}$$

3.4. Boundary conditions

We imposed U as the top lid wall velocity and $u = v = 0$ for other walls, also in x and y direction, velocity components are u and v, and temperature gradients are $T_x|_{x=0}$ $T_x|_{x=L}$, $T_y|_{y=0}$ & $T_y|_{y=L}$ respectively. Whereas the characteristics height is denoted by H and L is related to the characteristics length of the lid-driven cavity. As buoyancy force effects are negligible due to the top lid generating viscous heating, therefore it is excluded from analysis which is related to the heat transfer. The thermal energy equation does not include the Boussinesq approximation, hence, there is no convection taking place between the bottom fixed lid and the top moving lid [38, 39, 40, 41].

4. Methodology

The governing equations for the current study have been written out in the dimensionless form as follows, taking into account the various assumptions that have been discussed thus far:

4.1. Vorticity Stream function

The Vorticity Stream function equation can be founded by taking the curl of the equation (2):

$$\underbrace{\bigtriangledown \times \frac{\partial \overline{U}}{\partial t}}_{Temporal} + \underbrace{\bigtriangledown \times (\overline{U}.\bigtriangledown)\overline{U}}_{Convective} = -\underbrace{\bigtriangledown \times \frac{1}{\rho_0} \bigtriangledown \mathbb{P}}_{Pressure} + \underbrace{\nu \bigtriangledown \times \bigtriangledown^2 \overline{U}}_{Viscous}. \tag{18}$$

The following is one possible introduction to the stream function. As an added bonus, the vorticity can be described as follows:

$$u = \frac{\partial \psi}{\partial y}, \quad v = -\frac{\partial \psi}{\partial x}, \ \& \ \omega = \frac{\partial v}{\partial x} - \frac{\partial u}{\partial y}. \tag{19}$$

Consider term-by-term analogy, with reference to equation (18), we have

Temporal:

$$\bigtriangledown \times \frac{\partial \overline{U}}{\partial t} = \frac{\partial}{\partial t}(\bigtriangledown \times \overline{U}) = \frac{\partial}{\partial t}\vec{\omega}.$$

Convective:

$$\left.\begin{aligned} \bigtriangledown \times (\overline{U}.\bigtriangledown)\overline{U} &= \bigtriangledown \times \underbrace{(\frac{1}{2}\bigtriangledown(\overline{U}.\overline{U}) - \overline{U} \times \vec{\omega})}_{\text{Vector Identity}}, \\ &= \underbrace{\bigtriangledown \times \bigtriangledown}_{=0}(\frac{1}{2}(\overline{U}.\overline{U}) - \bigtriangledown \times (\overline{U} \times \vec{\omega}), \\ &= (\overline{U}.\bigtriangledown)\vec{\omega} - (\vec{\omega}.\bigtriangledown)\overline{U} + \vec{\omega}\underbrace{(\bigtriangledown.\overline{U})}_{\text{CE=0}}. \end{aligned}\right\}$$

Pressure:

$$\bigtriangledown \times \frac{1}{\rho_0} \bigtriangledown \mathbb{P} = \underbrace{\bigtriangledown \times \bigtriangledown}_{=0}(\frac{1}{\rho_0}\mathbb{P}) = 0.$$

Viscous:

$$\bigtriangledown \times (\nu \bigtriangledown^2 \overline{U}) = \nu \bigtriangledown^2 (\bigtriangledown \times \overline{U}) = \nu \bigtriangledown^2 \overrightarrow{\omega}.$$

Hence, recombining the temporal, convective, pressure, and viscous terms to get the following vorticity transport equation;

$$\frac{\partial \overrightarrow{\omega}}{\partial t} + (\overline{U}.\bigtriangledown)\overrightarrow{\omega} = (\overrightarrow{\omega}.\bigtriangledown)\overline{U} + \nu(\bigtriangledown^2 \overrightarrow{\omega}) \tag{20}$$

$$\begin{cases} \nabla^2 \psi = -\omega \\ \frac{\partial \psi}{\partial y}\frac{\partial \omega}{\partial x} - \frac{\partial \psi}{\partial x}\frac{\partial \omega}{\partial y} = \frac{\mu_{nf}}{\nu_f \rho_{nf}}\nabla^2 \omega + (\frac{\partial \Theta}{\partial y})\frac{Ra}{Pr\beta_f \rho_{nf}}((1-\varphi)\rho_f \beta_f + \varphi \rho_s \beta_s) \\ \frac{\partial \psi}{\partial y}\frac{\partial \Theta}{\partial x} - \frac{\partial \psi}{\partial x}\frac{\partial \Theta}{\partial y} = \frac{\alpha_{nf}}{\alpha_f Pr}\nabla^2 \Theta \end{cases} \tag{21}$$

4.2. Finite Volume (FV) approach

Transformation of PDEs into a system of linear algebraic equations can be done with the help of the finite volume technique which is quite well structured for simulations of fluid flow problems. Such a technique is distinctive and contains mostly two stages. In the first step, transformation can be performed by finding the integral to the differential equation which involves changing the volume and surface integrals into discrete algebraic relations over the elements. In the second step, interpolation profile assumption can be chosen to approximate the changes in the variables which exist within the confined volume and related surface values of the variables to their cell values can be transformed into algebraic relations. The selected approximations after these two steps provide a solid foundation for the accuracy and robustness of the resulting technique [39, 40, 41]. Let us focus on the discretization of the various parts of the general conservation equations.

$$\frac{\partial}{\partial t}(\rho \varphi) + \bigtriangledown.(\rho V \varphi) = \bigtriangledown.(\bigtriangledown \varphi) + S_{source} \tag{22}$$

$$\int_V \frac{\partial}{\partial t}(\varphi)dV = -\int_V \bigtriangledown.(\mathbf{u}\varphi)dV + \int_V \bigtriangledown.(k \bigtriangledown \varphi)dV + \int_V S^{\varphi}dV \tag{23}$$

Convert all fluxes to surface integrals by Gauss Divergence theorem,

$$\int_V \frac{\partial}{\partial t}(\varphi)dV \approx \frac{\partial \varphi_c}{\partial t}\bigtriangledown V_c$$

$$\int_V \bigtriangledown.(\mathbf{u}\varphi)dV = \int_{surface}(\mathbf{u}\varphi).\mathbf{n}ds = \sum f_1, f_{2,\ldots}\int_{s_i}(\mathbf{u}\varphi).\mathbf{n}ds_i$$

for $\mathbf{u} = (u, v)$

$$\int_V \bigtriangledown.(u\varphi)dV = \int_{fe} u\varphi ds_e - \int_{fe} \mathbf{u}\varphi ds_w + \int_{fe} v\varphi ds_n - \int_{fe} v\varphi ds_s \tag{24}$$

$$\int_V \bigtriangledown.(\mathbf{u}\varphi)dV = (u\varphi)_e.n_e\Delta s_e + (u\varphi)_w.n_w\Delta s_w + (v\varphi)_n.n_n\Delta s_n + (v\varphi)_s.n_s\Delta s_s \tag{25}$$

$$\frac{\partial \varphi_c}{\partial t}\Delta V_c = (u\varphi)_e\Delta y + (u\varphi)_w\Delta y + (v\varphi)_n\Delta x + (v\varphi)_s\Delta x$$

$$\frac{\partial \varphi_c}{\partial t} = \frac{(u\varphi)_e - (u\varphi)_w}{\Delta x} + \frac{(v\varphi)_n - (v\varphi)_s}{\Delta y}$$

$$\left.\begin{aligned} \frac{\partial \varphi_c}{\partial t}\Delta V_c = k \bigtriangledown . \bigtriangledown \varphi = k \sum f_1, f_2, ... \bigtriangledown \varphi_f . n_f \Delta S_f \\ = \bigtriangledown \varphi_e . n_e \Delta S_e + \bigtriangledown \varphi_w . n_w \Delta S_w + \bigtriangledown \varphi_n . n_n \Delta S_n + \bigtriangledown \varphi_s . n_s \Delta S_s \end{aligned}\right\} \tag{26}$$

$$\frac{\partial \varphi_c}{\partial t}\Delta x \Delta y = \frac{\partial \varphi}{\partial x}|_e \Delta y - \frac{\partial \varphi}{\partial x}|_w \Delta y + \frac{\partial \varphi}{\partial y}|_n \Delta x - \frac{\partial \varphi}{\partial y}|_s \Delta x$$

$$\frac{\partial \varphi_c}{\partial t} = \frac{\frac{\partial \varphi}{\partial x}|_e \Delta y - \frac{\partial \varphi}{\partial x}|_w \Delta y}{\Delta x} + \frac{\frac{\partial \varphi}{\partial y}|_n \Delta x - \frac{\partial \varphi}{\partial y}|_s \Delta x}{\Delta y} \tag{27}$$

The mass conservation equation is,

$$\int_{surface} \mathbf{u}.\mathbf{n} ds = \sum_{f_1, f_2, ...} \int_{s_i} \mathbf{u}.\mathbf{n} ds_i = 0,$$

for $\mathbf{u} = (u, v)$

$$\int_{surface} \mathbf{u}.\mathbf{n} ds \approx u_e \Delta y - u_w \Delta y + u_n \Delta x - u_s \Delta x \tag{28}$$

The x-directional pressure gradient is,

$$\frac{1}{\rho} \int_{surface} P.n_x ds \approx \frac{1}{\rho}(P_e \Delta y - P_w \Delta y), \tag{29}$$

the y-directional pressure gradient is,

$$\frac{1}{\rho} \int_{surface} P.n_y ds \approx \frac{1}{\rho}(P_n \Delta x - P_s \Delta x). \tag{30}$$

4.2.1. Implementation strategy:

We introduced cell-centered indexing such that scalar quantities are placed at the natural cell centers which are referred to as scalar volumes, also velocities and momentum have their own control volumes which are centered at the faces of the scalar volumes aligned for structured uniform grid [39, 40, 42, 43, 44].

1. Firstly, the continuity equation (3) can be read as:

$$\frac{u_e - u_w}{\Delta x} + \frac{u_n - u_s}{\Delta y} = 0$$

$$\frac{u_{i+1,j} - u_{i,j}}{\Delta x} + \frac{u_{i,j+1} - u_{i,j}}{\Delta y} = 0$$

2. Secondly, x-momentum convective flux in equation (17) can be read as:

$$\oint_S u\mathbf{u}.\mathbf{n} ds \approx (uu)_e \Delta y - (uu)_w \Delta y + (vu)_n \Delta x - (vu)_s \Delta x$$

$$\left.\begin{aligned} u_e \approx \tfrac{1}{2}(u_{i+1,j} + u_{i,j}) \\ u_w \approx \tfrac{1}{2}(u_{i,j} + u_{i-1,j}) \\ u_n \approx \tfrac{1}{2}(u_{i,j+1} + u_{i,j}) \\ u_s \approx \tfrac{1}{2}(u_{i,j} + u_{i,j-1}) \end{aligned}\right\} \quad \& \quad \left.\begin{aligned} v_n \approx \tfrac{1}{2}(v_{i-1,j+1} + v_{i,j+1}) \\ v_s \approx \tfrac{1}{2}(v_{i-1,j} + v_{i,j}) \end{aligned}\right\} \tag{31}$$

3. Thirdly, y-momentum convective flux in equation (17) can be read as:

$$\oint_S v\mathbf{u}.\mathbf{n}ds \approx (uv)_e\Delta y - (uv)_w\Delta y + (vv)_n\Delta x - (vv)_s\Delta x$$

$$\left.\begin{array}{l} v_e \approx \frac{1}{2}(v_{i,j} + v_{i+1,j}) \\ v_w \approx \frac{1}{2}(v_{i,j} + v_{i-1,j+1}) \\ v_n \approx \frac{1}{2}(v_{i,j} + v_{i,j+1}) \\ v_s \approx \frac{1}{2}(v_{i,j} + v_{i,j-1}) \end{array}\right\} \;\&\; \left\{\begin{array}{c} u_e \approx \frac{1}{2}(u_{i+1,j} + u_{i+1,j-1}) \\ u_w \approx \frac{1}{2}(u_{i,j} + u_{i,j-1}) \end{array}\right\} \tag{32}$$

4. Fourthly, x-directional diffusive flux in equation (17) can be read as:

$$\oint_S \nabla u.\mathbf{n}ds \approx \frac{\partial u}{\partial x}|_e\Delta y - \frac{\partial u}{\partial x}|_w\Delta y + \frac{\partial u}{\partial y}|_n\Delta x - \frac{\partial u}{\partial y}|_s\Delta x$$

$$\left.\begin{array}{l} \frac{\partial u}{\partial x}|_e \approx \frac{1}{\Delta x}(u_{i+1,j} - u_{i,j}) \\ \frac{\partial u}{\partial x}|_w \approx \frac{1}{\Delta x}(u_{i,j} - u_{i-1,j}) \\ \frac{\partial u}{\partial y}|_n \approx \frac{1}{\Delta y}(u_{i,j+1} - u_{i,j}) \\ \frac{\partial u}{\partial y}|_s \approx \frac{1}{\Delta y}(u_{i,j} - u_{i,j-1}) \end{array}\right\} \tag{33}$$

$$\oint_S \nabla v.\mathbf{n}ds \approx \frac{(u_{i+1,j} - u_{i,j} - u_{i,j} + u_{i-1,j})}{\Delta x^2} + \frac{(u_{i,j+1} - u_{i,j} - u_{i,j} + u_{i,j-1})}{\Delta y^2}$$

5. Fifthly, y-directional diffusive flux in equation (17) can be read as:

$$\oint_S \nabla v.\mathbf{n}ds \approx \frac{\partial v}{\partial x}|_e\Delta y - \frac{\partial v}{\partial x}|_w\Delta y + \frac{\partial v}{\partial y}|_n\Delta x - \frac{\partial v}{\partial y}|_s\Delta x$$

$$\left.\begin{array}{l} \frac{\partial v}{\partial x}|_e \approx \frac{1}{\Delta x}(v_{i+1,j} - v_{i,j}) \\ \frac{\partial v}{\partial x}|_w \approx \frac{1}{\Delta x}(v_{i,j} - v_{i-1,j}) \\ \frac{\partial v}{\partial y}|_n \approx \frac{1}{\Delta y}(v_{i,j+1} - v_{i,j}) \\ \frac{\partial v}{\partial y}|_s \approx \frac{1}{\Delta y}(v_{i,j} - v_{i,j-1}) \end{array}\right\} \tag{34}$$

$$\oint_S \nabla v.\mathbf{n}ds \approx \frac{(v_{i+1,j} - v_{i,j} - v_{i,j} + u_{i-1,j})}{\Delta x^2} + \frac{(v_{i,j+1} - v_{i,j} - v_{i,j} + v_{i,j-1})}{\Delta y^2}$$

6. Second lastly, x-directional pressure gradient in equation (17) can be read as:

$$\frac{1}{\rho}\int_{surface} P.n_x ds \approx \frac{1}{\rho\Delta x}(P_{i,j} - P_{i,j-1})$$

7. lastly, y-directional pressure gradient in equation (17) can be read as:

$$\frac{1}{\rho}\int_{surface} P.n_y ds \approx \frac{1}{\rho\Delta y}(P_{i,j} - P_{i,j-1})$$

4.3. Artificial Compressibility (AC) method

Let us consider the continuity equation in the following way,

$$\frac{1}{\delta}\frac{\partial p}{\partial t} + \frac{\partial u}{\partial x} + \frac{\partial v}{\partial y} = 0, \tag{35}$$

which leads to,

$$\frac{1}{\delta}\frac{p^{Advance} - p^{old}}{dt} + \frac{u_e - u_w}{\Delta x} + \frac{v_n - v_s}{\Delta y} = 0. \tag{36}$$

This method, known as artificial compressibility, uses a relatively straightforward strategy and is capable of dealing with some dimensionless numbers. A very precise velocity solution can be obtained using this method [44, 45].

5. Analysis

Numerical investigation of unsteady, incompressible, and two-dimensional lid-driven cavity flow with the aspect ratio $A = 1(1m \times 1m)$ is being done to understand the effect of viscous heating in both no-slip and free-slip Neumann boundary conditions in two case studies to characterize the flow field and temperature distribution with insulated walls. These examples, which feature laminar unsteady flow and different fluid parameters, are done iteratively.

5.1. Relevance of the grid size and time

The procedure continues until the analysis period, t = 2 s, has been reached (which is longer than the steady-state criterion). The Prandtl value is set at 6.2 for the grid independence test that is currently being conducted (pure water). A solid VF (0.1) of nanoparticles related to Copper (Cu) and a Rayleigh number (Ra) of 10^5 have been selected as the material. Computational work has been done on two different grid sizes, namely 30 by 30 and 72 by 72, and both of these grid sizes have been used. The computations have been done on a grid that is uniform throughout. Figures 2 & 3 show numerical results at grid sizes (30×30) & (72×72) with $Ra = 10^5$ for analysis at two different time period $2s$ and $20s$. It has been decided to take time step dt as 0.001. Figure 2(a) depicts the horizontal component of velocity with the main vortex, due to top lid velocity at $2m/s$ while Figure 3(a) represents results at $20m/s$. Also, Figures 2(b) & 3(b) depict the vertical component of velocity with two vortices at the top corners of the lid. Figures 2(c) & 3(c) depicts the distribution of the u-velocity in the vertical mid-plane as well as the v-velocity in the horizontal mid-plane. The kinetic energy profile can be visualized from Figures 2(d) & 3(d). The contour plot of the isotherms exhibits symmetry due to the bottom wall temperature distribution and vertical wall boundary conditions. The flow is mostly two counter-rotating circulating cells, regardless of Rayleigh number or solid volume fraction which can be seen from Figures 2(e), 3(e), 2(b) & 3(b). The kinetic energy profile has been taken into consideration from the center line in order to examine the outcomes of using different grid sizes and two distinct time levels, see Figures 2(f) & 3(f).

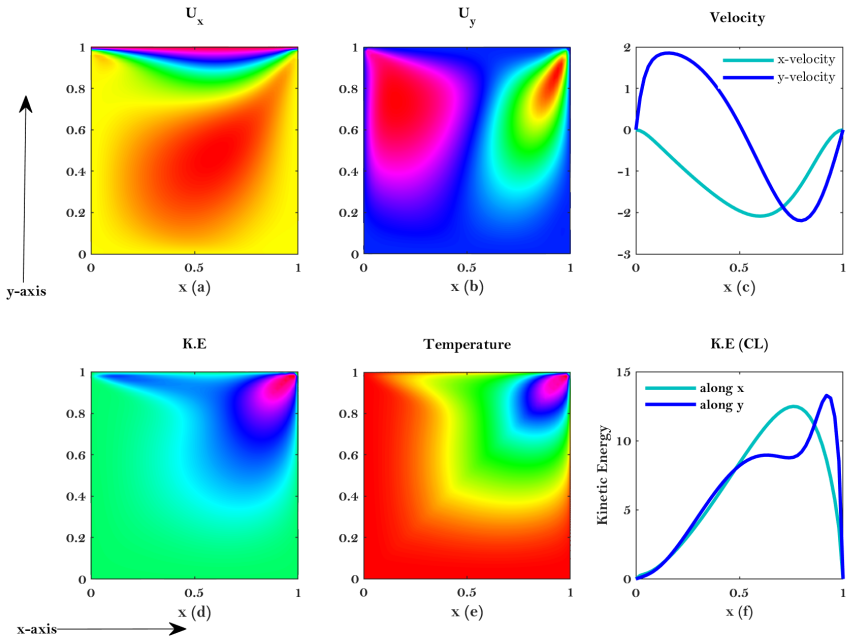

Figure 2: Depicts a lid-driven cavity model with $Ra = 10^5$, grid sizes (30×30), time step dt as 0.001 and top lid velocity is $2m/s$.

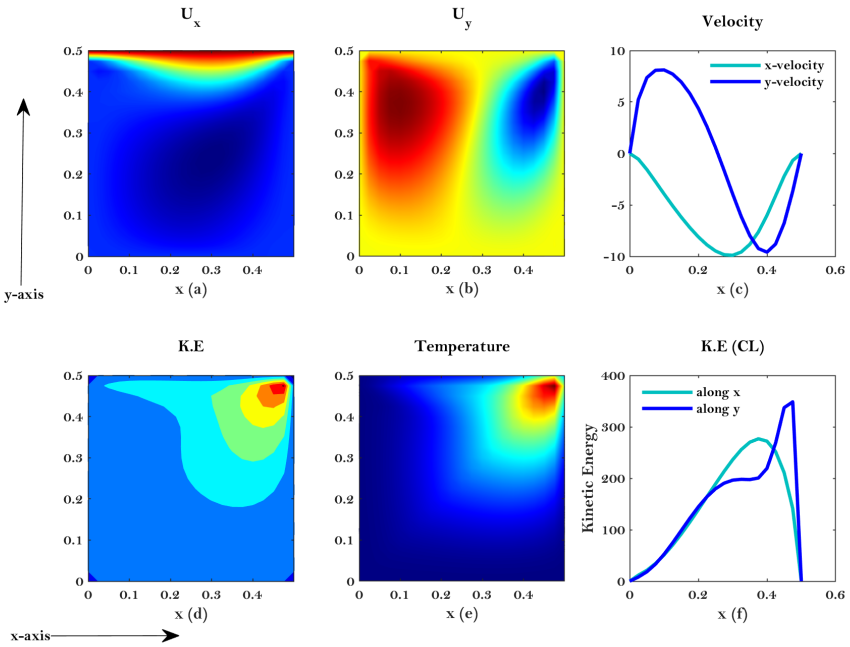

Figure 3: Depicts a lid-driven cavity model with $Ra = 10^5$, grid sizes (72×72), time step dt as 0.001 and top lid velocity is $20m/s$.

5.2. Vorticity stream function solution

An analytical asymptotic solution has been proposed by us for the problem of vorticity, and it is located close to the cavity's corners. In addition, using the finite volume technique, we determined a singularity-free boundary condition for the vorticity at the corners and the walls. Vorticity values at the wall utilizing either of the two numerical methodologies with the aforementioned detailed 4.2.1 & 4.3, the following expression should be used. The boundary conditions in each of those operations are affected in the following way: (φ, ω) related dimensionless boundary conditions: $\psi = 0$, for $x = 0, 1$

Transported quantities	**Equation of Vorticity**	**Energy Equation**
Quantity	ω	Θ
η	$\frac{Ra}{\rho_{nf}\beta_f Pr}((1-\varphi)\rho_f\beta_f + \varphi\rho_s\beta_s)$	$\frac{\mu_{nf}}{\nu_f\rho_{nf}}$
ε	0	$\frac{\alpha_{nf}}{\alpha_f Pr}$

Table 2: Shows transport system (17) & (21) presentation for different terms.

and $0 \leq y \leq 1$ as well as for $y = 0, 1$ and $0 \leq x \leq 1$. Figures 4(b) and 4(c) depict the value of ω and corresponding streamlines (SL) which is translated in terms of velocity along the x-direction u_x which can be seen from Figure 4(a). While Figures 4(e) and 4(f) depict the value of ψ and corresponding streamlines (SL) which is translated in terms of velocity along the y-direction U_y which can be seen from Figure 4(d).

The velocity profiles U_x and U_y from the mid line of cavity at $y = 0.005$ and $x = 0.005$ for various φ are presented in Figures 5(b) and 5(c). In point of fact, when Ra are set to 10^4 and $\varphi = 0\%$, the greatest values of vertical velocity have a variation of 14.23% [41, 42]. These discrepancies are shown to decrease with an increase in the Rayleigh number. In terms of plotting the temperature which is distributed, it is possible to see distinct variations in the isotherm contour plot, see Figure 5(e) when compared to the scenario in which $\varphi = 0\%$. When the percentage of solid particles in the total volume increases, the variations become more pronounced. Because of these changes, the presence of nanoparticles has a significant impact, see Figures 5(a,d & f).

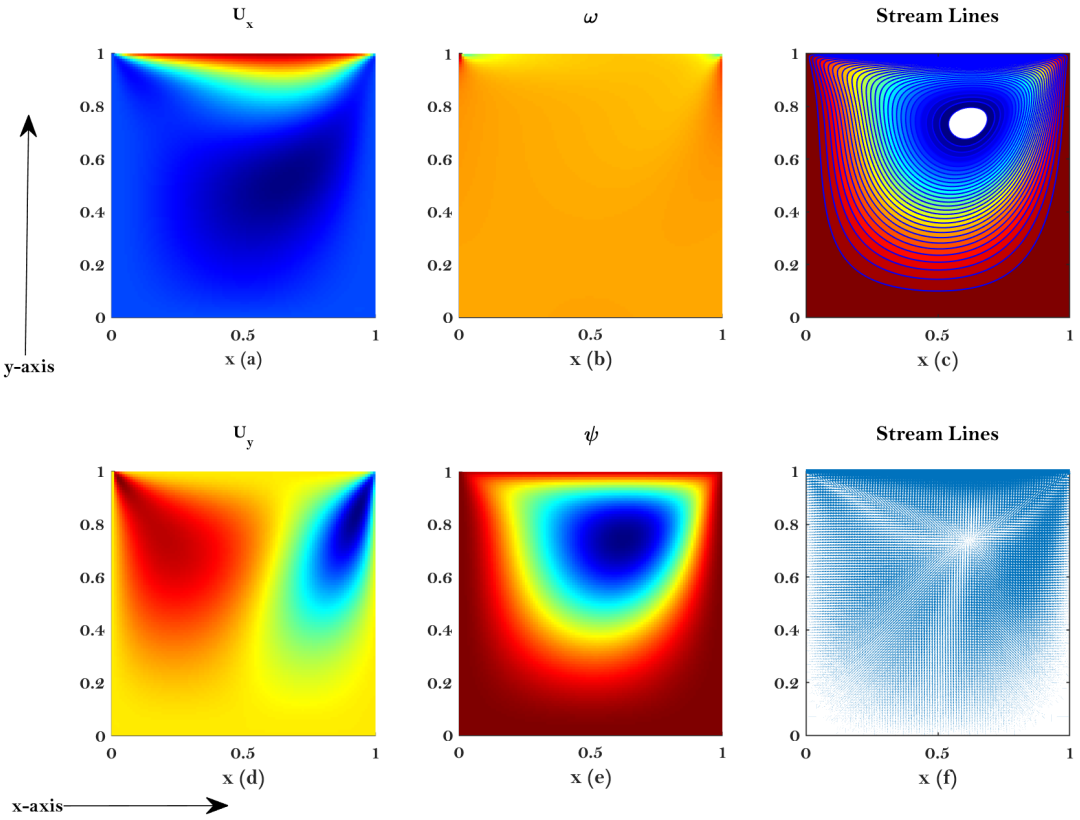

Figure 4: Depicts with $Ra = 10^4$, grid sizes (30×30) and $\varphi = 0\%$

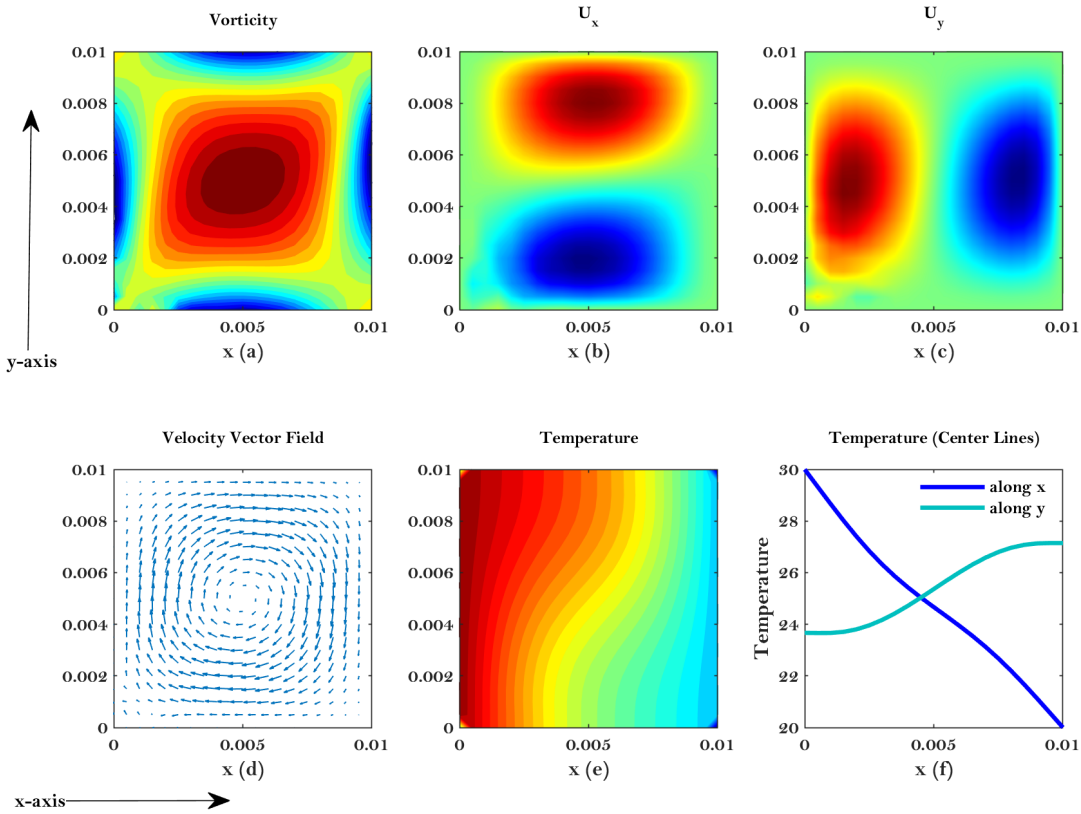

Figure 5: Depicts a lid-driven cavity model with $Ra = 10^4$, grid sizes (72×72) and $\varphi = 2\%$

5.3. Significance of φ & Ra

Figures 6(a-c) illustrate the distribution of heat transfer that occurs through the hot wall by plotting lines of the energy equation against different values of Rayleigh number Ra and volume fraction φ. Symmetric behavior of temperature is observed with regard to the plane $x = 0.005$ for each and every possible combination of Ra & φ. The amount of heat that is transferred through the hot wall is relatively modest when the Rayleigh number is low $(Ra = 5 \times 10^3)$ and $\varphi = 0\%$, therefore results in a minor curvature when $x = 0.005$ is reached. This curvature is because of the substantially higher intensity of the cells that rotate in the opposite direction to one another [41, 42, 44]. Because of the reduction in fluid velocity, the curvature at the center of the figure vanishes when is increased to a value of 0.1. The maximum amount of heat that can be transferred occurs at a φ value of 0.4%, and the amount of heat that can be transferred is increased [41, 42, 44]. On the curves corresponding to various values of Rayleigh numbers such as $Ra = 5 \times 10^4$ and $Ra = 5 \times 10^5$, with prominent heat transfer in the neighborhood of $x = 0.025$ and $x = 0.075$ is observed. Because the top lid is moving, the heat is generated there and is first concentrated in the top right corner. After that, the warmth gradually spreads to the cavity's right bottom corner as well as the rest of the space within it. The free-slip boundary condition, on the other hand, results in a temperature distribution that is less extreme overall. In contrast to the no-slip boundary condition, the free-slip boundary condition places additional constraints on the development of eddies. A comparison of temperature profiles is carried out for a variety of volume fractions and their respective values. The temperature profiles for both types of slip boundary conditions follow a similar trend at the point with the greatest value of the stream function, and the temperatures continue to rise. Hence, the fluid is able to freely slide over the wall or solid interface, and as a result, there is no possibility of frictional heat being generated at the wall. The reduced applied velocity on the top lid lowers the temperature profile and reduces the stream function distribution in the complete lid-driven flow as required by the governing system. The last component on the right-hand side of the thermal energy equation is significantly related to the stream function, therefore viscous heating will lower the temperature profile.

In addition to this, it is interesting to note that the steady-state period at the threshold of $error = 10^{-5}$ for all three instances such as for Ra has been reached for the fluid flow, indicated in Figure, it is not possible to see a steady-state condition for any of the three examples' temperature profiles 6(a-c). Therefore, the temperature profile rises in a quasi-linear manner, despite the fact that the equation (17) is an elliptic equation. It is possible to extrapolate the temperature profile at some particular position, or perhaps at any place within the cavity, which will continue to rise.

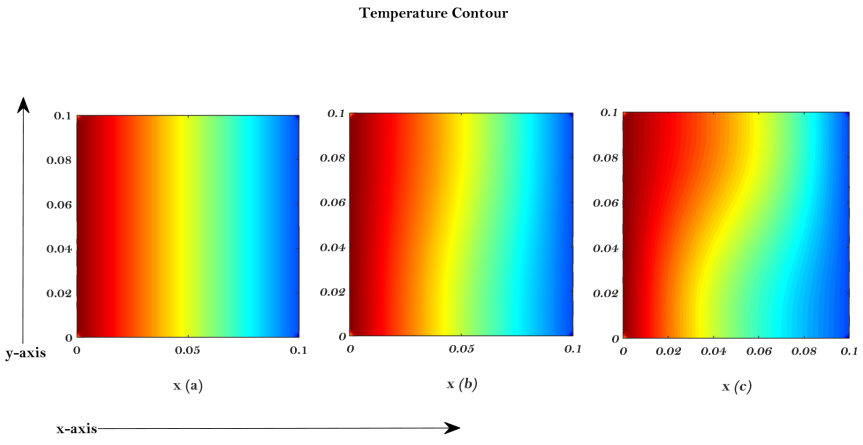

Figure 6: Depicts results for temperature with different values of Ra and φ.

6. Conclusion

The enhancement of heat transmission in a two-dimensional enclosure that is filled with nanofluids is investigated using computational methods in this study. A new artificial compressibility formulation was developed, and the effect of a thermal boundary condition was examined, for a range of Rayleigh numbers Ra and nanoparticle volume fractions φ. Because of the symmetry criterion that is enforced on the boundary of the bottom wall, the flow and temperature fields are symmetrical in the vicinity of the central plane of the enclosure. Following is a list of the primary inferences that can be derived from the outcomes of this work:

- New artificial compressibility concept matches prior studies. Different Rayleigh numbers validated our numerical coding [45].
- As the top lid moves, a constant heat flux is generated and supplied continually, resulting in a rising temperature profile in three of the cases. The temperature profiles of these test cases will continue to rise if the iteration time is increased to any other period. Because of this, a meteorite's surface temperature keeps rising as it falls through space, despite the fact that the meteorite's contact with the air during its fall generates only a negligible amount of heat due to friction or viscous heating [25, 42, 45].
- In addition to a lower Ra number and reduced thermal diffusivity, the free-slip effect of the fluid flow can also contribute to more uniform temperatures.
- A higher value of the Prandtl number (Pr), can lead to a more uniform temperature distribution within the cavity model.
- Despite the fact that the vorticity stream function technique is straightforward and adequate for explaining the Neumann boundary and the free-slip effect, this method can be used for problems with basic/complex geometry [36, 41, 42, 45].
- A study comparing the effects of nanoparticles with varying volume fraction and Rayleigh numbers Ra show that the nanoparticles significantly boost the heat transfer rate. Also, the concentration of copper (Cu) nanoparticles and the flow of the nanofluid both improve. This research will soon be expanded to include additional types of base fluids and nanoparticles, as well as additional sorts of geometry investigations [29, 32, 41, 44].
- Because the free-slip effect is considered to operate as a lubricant, it will cause the fluid to flow quicker than it would with the no-slip boundary, but the temperature distribution will be lower with the free-slip effect than it would be with the no-slip boundary [29, 32, 41, 45].
- Mathematical formulations of continuity, momentum, and boundary conditions regulate the physical design. Finite volume for a staggered grid combined with an artificial compressibility approach is used to solve the incompressible Navier Stokes equations for two-dimensional unsteady fluid flow in a square cavity. In all situations, a detailed analysis is done and contour plots are shown while line graphs show velocity components. Analysis of kinetic energy is performed. The results described in this study should benefit future research on fluid flow in industrial enclosures.

Conflicts of Interest

The authors declare no conflicts of interest regarding the publication of this article.

Author contributions statement

Writing-review & editing S. Hasnain; Methodology and Resources N. Odah; Data curation and visualization M. Saqib; Supervision Muhammad Farman. The final form of the article has been reviewed and approved by all the authors.

Data availability

The data that support the findings of this study are available within the article.

Funding

This research received no external funding.

[1] Shankar, PN and Deshpande, MD. Fluid mechanics in the driven cavity. Annual review of fluid mechanics, 2000, 32, 1, 93–136.

[2] Kawaguti, Mitutosi. Numerical solution of the Navier-Stokes equations for the flow in a two-dimensional cavity. Journal of the Physical Society of Japan, 1961, 16, 11, 2307–2315.

[3] Burggraf, Odus R. Analytical and numerical studies of the structure of steady separated flows. Journal of Fluid Mechanics, 1966, 24, 1, 113–151.

[4] Ghia, UKNG and Ghia, Kirti N and Shin, CT. High-Re solutions for incompressible flow using the Navier-Stokes equations and a multigrid method. Journal of computational physics, 1982, 48, 3, 387–411.

[5] Schreiber, Rob and Keller, Herbert B. Driven cavity flows by efficient numerical techniques. Journal of Computational Physics, 1983, 49, 2, 310–333.

[6] Chiang, TP and Sheu, WH. Numerical prediction of eddy structure in a shear-driven cavity. Computational Mechanics, 1997, 20, 4, 379–396.

[7] Deville, Michel and Lê, Thien-Hiep and Morchoisne, Yves. Numerical Simulation of 3-D Incompressible Unsteady Viscous Laminar Flows: A GAMM-Workshop. Vieweg+ Teubner Verlag, 2013, 48, 1, 1–7.

[8] Albensoeder, Stefan and Kuhlmann, Hendrik C. Accurate three-dimensional lid-driven cavity flow. Journal of Computational Physics, 2005, 206, 2, 536–558.

[9] Gupta, Murli M and Manohar, Ram P and Noble, Ben. Nature of viscous flows near sharp corners. Computers & Fluids, 1981, 9, 4, 379–388.

[10] Leriche, Emmanuel. Direct numerical simulation in a lid-driven cubical cavity at high Reynolds number by a Chebyshev spectral method. Journal of Scientific Computing, 2006, 27, 1–3, 335–345.

[11] Taylor, GI. Similarity solutions of hydrodynamic problem. Aeronautics and Astronautics, 1961, 4, 1, 21–28.

[12] Riedler, J and Schneider, W. Viscous flow in corner regions with a moving wall and leakage of fluid. Acta Mechanica, 1983, 48, 1–2, 95–102.

[13] Goodrich, John W and Gustafson, Karl and Halasi, Kadosa. Hopf bifurcation in the driven cavity. Journal of Computational Physics, 1990, 90, 1, 219–261.

[14] Patankar, Suhas V and Spalding, D Brian. A calculation procedure for heat, mass and momentum transfer in three-dimensional parabolic flows. Numerical prediction of flow, heat transfer, turbulence and combustion, Elsevier, 1983, USA.

[15] Acharya, S and Baliga, BR and Karki, Kailash and Murthy, JY and Prakash, C and Vanka, Surya Pratap. Pressure-based finite-volume methods in computational fluid dynamics. J. Heat Transfer, 2007, 129, 4, 407–424.

[16] Bruneau, Charles-Henri and Jouron, Claude. An efficient scheme for solving steady incompressible Navier-Stokes equations. Journal of Computational Physics, 1990, 89, 2, 389–413.

[17] Thai-Quang, N and Le-Cao, K and Mai-Duy, N and Tran-Cong, T. A high-order compact local integrated-RBF scheme for steady-state incompressible viscous flows in the primitive variables. CMES Computer Modeling in Engineering and Sciences, 2012, 84, 6, 528–557.

[18] Smith, Jason Richard. An accurate Navier-Stokes solver with an application to unsteady flows. Graduate Theses, Dissertations, and Problem Reports, West Virginia University, 1997. https://researchrepository.wvu.edu/etd/9797

[19] Farooq, Umar and Khan, Shan Ali and Chan, Tzu-Chi and Naqvi, Syed Muhammad Raza Shah and Waqas, Hassan and Ullah, Aman. Heat Transfer of Casson Nanofluid Flow Between Double Disks: Using Buongiorno Model. Journal of Nanofluids, 2024, 13, 3, 783–794.

[20] Farooq, Umar and Riaz, Hafiz Hamza and Munir, Adnan and Zhao, Ming and Tariq, Ammar and Islam, Mohammad S. Application of heliox for optimized drug delivery through respiratory tract. Physics of Fluids, 2023, 35, 10, 1–13.

[21] Khanafer, Khalil and Vafai, Kambiz and Lightstone, Marilyn. Buoyancy-driven heat transfer enhancement in a two-dimensional enclosure utilizing nanofluids. International journal of heat and mass transfer, 2003, 46, 19, 3639–3653.

[22] Lee, S and Choi, SU-S and Li, S, and Eastman, JA. Measuring thermal conductivity of fluids containing oxide nanoparticles. Journal of Heat Transfer, 1999, 121, 2, 1–13.

[23] Xie, Hua-qing and Wang, Jin-chang and Xi, Tong-geng and Liu, Yan. Thermal conductivity of suspensions containing nanosized SiC particles. International Journal of Thermophysics, 2002, 23, 571–580.

[24] Wen, Dongsheng and Ding, Yulong. Experimental investigation into convective heat transfer of nanofluids at the entrance region under laminar flow conditions. International journal of heat and mass transfer, 2004, 47, 24, 5181–5188.

[25] Xuan, Yimin and Li, Qiang. Investigation on convective heat transfer and flow features of nanofluids. J. Heat transfer, 2003, 125, 1, 151–155.

[26] Naramgari, Sandeep and Sulochana, C. MHD flow of dusty nanofluid over a stretching surface with volume fraction of dust particles. Ain Shams Engineering Journal, 2016, 7, 2, 709–716.

[27] Zhou, Wenning and Yan, Yuying and Liu, Xunliang and Chen, Hongxia and Liu, Baiqian. Lattice Boltzmann simulation of mixed convection of nanofluid with different heat sources in a double lid-driven cavity. International Communications in Heat and Mass Transfer, 2018, 97, 39–46.

[28] Incropera, Frank P and DeWitt, David P and Bergman, Theodore L and Lavine, Adrienne S and others. Fundamentals of heat and mass transfer, 6, Wiley New York, USA.

[29] Rahman, MM and Öztop, Hakan F and Rahim, NA and Saidur, Rahman and Al-Salem, Khaled. MHD mixed convection with joule heating effect in a lid-driven cavity with a heated semi-circular source using the finite element technique. Numerical Heat Transfer, Part A: Applications, 2011, 60, 6, 543–560.

[30] Anderson, John David. Modern compressible flow: with historical perspective, 12, 1990, McGraw-Hill New York, USA.

[31] Wakif, A and Animasaun, IL and Narayana, PV Satya and Sarojamma, G. Meta-analysis on thermo-migration of tiny/nano-sized particles in the motion of various fluids. Chinese Journal of Physics, 2020, 68, 293–307.

[32] Griffiths, D Vaughan and Smith, Ian Moffat. Numerical methods for engineers, 2006, Chapman and Hall/CRC, UK.

[33] Saqib, Sana Ullah and Farooq, Umar and Fatima, Nahid and Shih, Yin-Tzer and Mir, Ahmed and Kolsi, Lioua. Novel Recurrent neural networks for efficient heat transfer analysis in radiative moving porous triangular fin with heat generation. Case Studies in Thermal Engineering, 2024, 64, 105516.

[34] Farooq, Umar and Saqib, Sana Ullah and Khan, Shan Ali and Liu, Haihu and Fatima, Nahid and Muhammad, Taseer and Faiz, Zeshan. Mathematical modeling of radiative nanofluid flow over nonlinear stretching sheet using artificial neural networks and Levenberg-Marquardt scheme: Applications in solar thermal energy. Solar Energy Materials and Solar Cells, 2025, 281, 113265.

[35] Ben-Cheikh, Nader and Chamkha, Ali J and Ben-Beya, Brahim and Lili, Taieb. Natural convection of water-based nanofluids in a square enclosure with non-uniform heating of the bottom wall. Scientific Research Publishing, 2013, 1, 1–7.

[36] Tiwari, Raj Kamal and Das, Manab Kumar. Heat transfer augmentation in a two-sided lid-driven differentially heated square cavity utilizing nanofluids. International Journal of heat and Mass transfer, 2007, 50, 9–10, 2002–2018.

[37] Abu-Nada, Eiyad. Application of nanofluids for heat transfer enhancement of separated flows encountered in a backward facing step. International Journal of Heat and Fluid Flow, 2008, 29, 1, 242–249.

[38] Brinkman, Hendrik C. The viscosity of concentrated suspensions and solutions. The Journal of chemical physics, 1952, 20, 4, 571–571.

[39] Al-Atawi, Nawal Odah and Hasnain, Shahid and Saqib, Muhammad and Mashat, Daoud S. Significance of Brinkman and Stokes system conjuncture in human knee joint. Scientific Reports, 2022, 12, 1, 18992.

[40] Hasnain, Shahid and Abbas, Imran and Al-Atawi, Nawal Odah and Saqib, Muhammad and Afzaal, Muhammad F and Mashat, Daoud S. Knee synovial fluid flow and heat transfer, a power law model. Scientific Reports, 2023, 13, 1, 18184.

[41] Zaydan, Mostafa and Yadil, Naoufal and Boulahia, Zoubair and Wakif, Abderrahim and Sehaqui, Rachid. Fourth-Order Compact Formulation for the Resolution of Heat Transfer in Natural Convection of Water-Cu Nanofluid in a Square Cavity with a Sinusoidal Boundary Thermal Condition. World Journal of Nano Science and Engineering, 2016, 6, 2, 70–89.

[42] Wong, HF and Sohail, Muhammad and Siri, Zailan and Noor, Noor Fadiya Mohd. Numerical solutions for heat transfer of an unsteady cavity with viscous heating. Computers, Materials & Continua, 2021, 68, 1, 319–336.

[43] Gupta, Murli M. High accuracy solutions of incompressible Navier-Stokes equations. Journal of Computational Physics, 1991, 93, 2, 343–359.

[44] Demir, Hüseyin and Sahin, Serpil. Numerical investigation of a steady flow of an incompressible fluid in a lid driven cavity. Turkish Journal of Mathematics and Computer Science, 2016, 1, 14–23.

[45] Shen, Jie. Pseudo-compressibility methods for the unsteady incompressible Navier-Stokes equations. Proceedings of the 1994 Beijing symposium on nonlinear evolution equations and infinite dynamical systems, 1997, 68–78.